

Unclonable Anti-Counterfeiting Labels Based on Microlens Arrays and Luminescent Microparticles

Vinay Kumar, Stephan Dottermusch, Ngei Katumo, Aditya Chauhan, Bryce S. Richards, and Ian A. Howard*

Micron-scale randomness during manufacturing can create unique and unclonable anti-counterfeiting labels. The security of such labels typically comes at the expense of complex hardware being required for authentication. This work demonstrates unclonable labels that can be authenticated using simple hardware such as a standard light-emitting diode and smartphone camera. These labels consist of a microlens array laminated to a luminescent-microparticle-doped polymer film, and thereby present a new method of making microscopic particle distributions visible on the macroscopic scale. The current novel design offers two significant practical advantages: 1) use of an incoherent source; and 2) authentication independent of the detector position. A comparison of 100 test images against 100 different reference images (total of 10,000 comparisons out of which 100 should authenticate and 9900 should not), demonstrates that authentication is robust with an estimated probability of a false positive on the order of 10^{-15} . Finally, a proof-of-concept is demonstrated through successful authentication of a label by a single smartphone, simultaneously providing both excitation and detection on the front side of the label.

Union (EU), counterfeit products traded in 2019 alone were valued at USD 134 billion (5.8% of the EU imports).^[1] Beyond economic consequences, counterfeiting can also endanger human lives, for example, by producing unsafe or ineffective pharmaceutical products^[3] and compromising safety standards.^[4] To combat counterfeiting, an approach gaining significant interest is to uniquely identify products with unclonable labels, often referred to as physically-unclonable functions (PUFs). Unclonable labels rely on micron-scale randomness in the manufacturing process to produce a series of unique labels that are highly resistant to forgery.^[5]

The unique physical characteristics of each unclonable label are characterized after manufacture and converted to digital codes that are stored in a database. These labels are then attached to a product before it enters the supply chain. Along the chain, any actor (e.g., a distributor or

1. Introduction

Counterfeiting is a growing challenge for industries and governments worldwide. In 2019, the loss to the global economy due to counterfeit products was USD 464 billion (2.5% of the international trade),^[1] it has been estimated that this value will reach USD (1.9–2.81) trillion by 2022.^[2] Within the European

consumer) with the appropriate hardware can check the label's authenticity by sending the results of their test characterization to compare against the information stored in the database. We note here that a plain serial number can also be attached to the unclonable label so that the test characterization image need only be compared against the references for a given label instead of the complete database. This vastly reduces the number of computationally costly test–reference comparisons that need to be made and therefore drastically reduces authentication time.^[3b,6] A schematic of the process described above is presented in Figure S1, Supporting Information. At a system level, such unique identifiers also combat forgery. Given the database and authentication requests are centrally managed, and the authentication requests come from trusted parties (the consumer is not motivated to try to attack the system to achieve a false authentication), if a few single labels are cloned this could be identified by excess requests to authenticate the same label from unexpected geographic locations. The few compromised unique labels could then be flagged as inauthentic. Of course, this is a general feature of serial marking, but one that can be used to further reduce the incentive for embarking on the laborious task of attempting to clone a single label of the design introduced below.

The seminal work of Pappu et al. in 2002 was a key event in the launch of interest in unclonable anti-counterfeiting labels.^[7]

V. Kumar, S. Dottermusch, N. Katumo, A. Chauhan, B. S. Richards, I. A. Howard

Institute of Microstructure Technology
Karlsruhe Institute of Technology
Hermann-von-Helmholtz-Platz 1, 76344
Eggenstein-Leopoldshafen, Germany
E-mail: ian.howard@kit.edu

B. S. Richards, I. A. Howard
Light Technology Institute
Karlsruhe Institute of Technology
Engesserstrasse 13, Karlsruhe 76131, Germany

 The ORCID identification number(s) for the author(s) of this article can be found under <https://doi.org/10.1002/adom.202102402>.

© 2022 The Authors. Advanced Optical Materials published by Wiley-VCH GmbH. This is an open access article under the terms of the Creative Commons Attribution License, which permits use, distribution and reproduction in any medium, provided the original work is properly cited.

DOI: 10.1002/adom.202102402

Therein, they created anti-counterfeiting labels that were based on the random distribution of scattering microparticles in a polymer layer.^[7] When exposed to coherent radiation, the scattered light from the microparticles creates interference patterns that can be observed on the macroscopic scale (i.e., using a standard camera). This interference pattern is unique, as it is based on the unique and random distribution of the scattering centers. The observed interference pattern further depends on the properties of the coherent radiation impinging on the scattering centers and the position of the detector relative to the scattering centers. Thus, a single label generates not only a single unique pattern but also a variety of unique patterns that depend on the conditions of the laser excitation and on the exact position of the detector relative to the anti-counterfeiting label. For the case of coherent radiation, the speckle pattern will be changed with incidence angle along with other factors such as collimation, precise wavelength, and spatial coherence length. The different interference patterns from a single label at different stimulation conditions make the label even more difficult to forge. The authors demonstrated this by recording the different interference patterns at different angles of incidence (AOIs) of the laser with respect to the label.^[7] However, the dependence of the speckle pattern on so many variables introduces the practical challenge of needing to accurately control over all these variables in every authentication setup thus, increasing system cost and complexity. Herein, we also present an anti-counterfeiting label whose optical properties are determined by micron-scale randomness but easily visible at the macroscale. However, the novel labels presented herein allow the use of noncoherent light from a standard light-emitting diode (LED) as the excitation source. Further, the authentication of the optical response does not require a precise control of the camera position. Both these factors have significant impact in terms of practical application. Reliance on scatter from laser excitation requires that each authentication system has an equivalent coherent source. This adds significant complexity in terms of implementation. Creating multiple authentication units with a consistent (and stable) emission wavelength and coherence properties using low-cost semiconductor lasers is not trivial. The ability to use LEDs, including those already ubiquitous in smartphone flashlights, easily removes this barrier. Next, the independence of the unique pattern with respect to the detector position eliminates another major drawback for a field-based authentication apparatus.

As schematically introduced in **Figure 1**, our unclonable labels are based on a microlens array (MLA) laminated onto a polymer layer doped with luminescent microparticles. Each lens in the MLA focuses the incident light to a point in the label that may or may not coincide with a phosphor particle (Figure 1a). If the focus is occupied by a phosphor microparticle, the emission from this microparticle will be much brighter relative to other phosphor particles not in a focus. The random locations of the microparticle phosphors lead to a random subset of the foci coinciding with a microparticle and therefore, a pattern of bright emission points resembling the stars in the night sky. This unique “constellation” of bright emission points can be easily imaged by a smartphone camera, as shown in Figure 1b. We note that the position of the camera does not fundamentally affect the pattern observed. If the camera is moved or rotated, a different projection

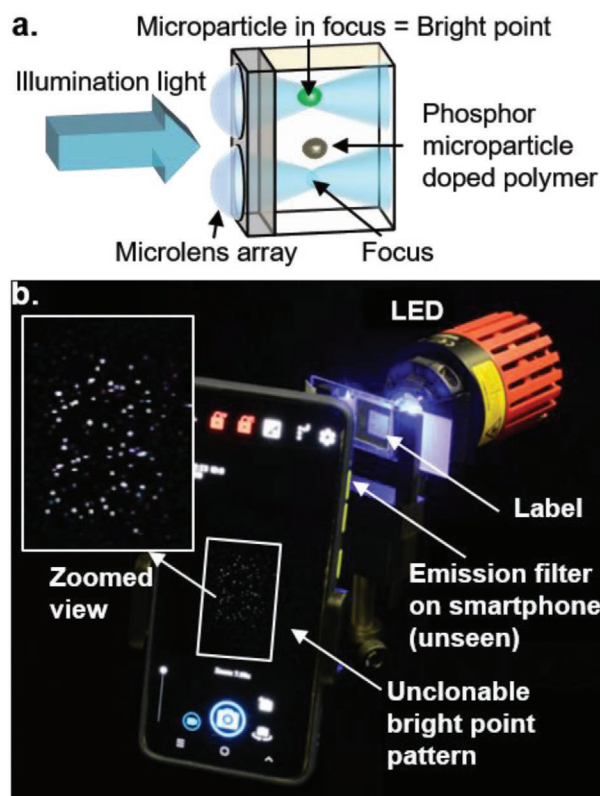


Figure 1. Anti-counterfeiting label concept based on microlens array laminated to a polymer layer doped with microparticle phosphors. a) The label consists of a microlens array attached to a polymer layer with phosphor microparticles randomly distributed through its bulk. When illuminated, each microlens focuses the light impinging upon it into a focal volume. If a focal volume is occupied by a phosphor microparticle, the emission from such a microparticle is much brighter than that from out-of-focus particles. This leads to a pattern of bright emission points. b) The constellation-like pattern of bright emission points from microparticles lying in foci can be easily detected with low-cost hardware. In this example, a blue LED excites the label whose emission is detected with a smartphone camera. In the current instance, an optical long-pass filter is placed before the smartphone camera to reject the excitation light.

of the emission pattern is recorded but an appropriate transformation of the test relative to the reference image during authentication satisfactorily removes any influence of camera position (see Section S2, Supporting Information). The AOI of the incident light, on the other hand, does shift the locations of the foci under the microlenses, and therefore, the emission pattern. Sufficiently different AOIs create different constellations from the same label. The utilization of two or more distinct emission patterns collected at different AOIs for authentication is key for the security of the proposed design (which only detects macroscopic features). A single bright point pattern could be rather easily recreated by low-resolution printing of an appropriate pattern with a luminescent ink (without a microlens array). Such an attack would yield the same pattern as one AOI. However, reproducing the different emission patterns at multiple angles would require true reproduction of the random microparticle positions relative to the microlens array with sub-100 μm accuracy, a challenging technical proposition (and unrealistic on a large scale given the cost and time needed).

Before embarking on the results and discussion relating to our new labels, we wish to highlight the state-of-art regarding unclonable anti-counterfeiting labels to put the present study in context. Recent reviews of the subject by Sørensen et al. and Jin et al. are recommended to the interested reader for a more complete presentation.^[5,8] Shortly after the orientation-sensitive physical unclonable label,^[7] Cowburn and coworkers showed that the random surface texture of objects (such as paper documents) can itself enable forgery-proof authentication.^[9] The authors developed an apparatus consisting of an excitation laser and several photodiodes whose signals are monitored as a surface (such as a paper document or plastic card) are swept underneath.^[9a,b] Later, Toreini and coworkers demonstrated through images captured by a standard camera that transmission of light through a piece of paper is sufficient to uniquely identify the paper.^[9c] Image analysis has also been developed for individually molded plastic parts,^[10] metal parts,^[11] and barcodes.^[12] Also, several new materials and approaches have been developed for unclonable anti-counterfeiting. For example, in 2014 Kim and coworkers showed that unique unclonable labels can be made by the random formation of networks of silver nanowires in a polymer matrix, which could be authenticated under an optical microscope.^[13] In 2015, Bae et al. demonstrated that unique, unclonable patterns of surface wrinkles are created upon drying of rigid-shell soft-core microparticles and that these can be authenticated using confocal laser scanning microscopy.^[14] A year later, Zheng et al. used fluorescein-embedded Ag@SiO₂ plasmonic nanoparticles to create unique and random emission point patterns (emission from individual particles) that were observable using a fluorescence microscope.^[15] Smith et al. used microscopy to compare and authenticate the unique point-patterns created by the scattering of drop-cast plasmonic Au nanoparticles.^[16] Liu et al. demonstrated in 2019 that by introducing PMMA nanoparticles to the ink-receiving layer before ink-jet printing luminescent quantum dots, pinning points are created around which unique micron-scale patterns of the luminescent quantum dots are generated during drying.^[17] Also, recently Leem et al. developed luminescent patterns of fluorescent silk microparticles embedded in a silk film to create edible, unclonable fluorescent labels that can be directly attached to pharmaceuticals. These were read out using a scientific camera with a zoom lens and liquid-crystal-based tunable filter.^[18] Carro-Temboury et al. recently demonstrated that zeolite cubes on a scale of 10 μm can be loaded with a mixture of emissive trivalent lanthanide ions such as europium, terbium, and dysprosium that exhibit red, green, and blue emission, respectively.^[6] The different colored emissions can be imaged using an optical microscope to reveal the random loading of each zeolite crystal, again leading to an unclonable label.^[6] The same group followed up this work with an excellent example of unique unclonable tags based on imaging random distributions of micron-sized scattering or luminescent particles on a surface. The imaging was done using either a microscope or with a smartphone camera equipped with a clip-on macro lens.^[19] This latter work is especially relevant to the present study in that it shares the goal of enabling a wider-spread uptake of unclonable labels by allowing simpler hardware—based around ubiquitous smartphones—to authenticate the labels. The work on creating and

characterizing unique optical point patterns continues to rapidly progress, with Kayaci and coworkers converting a thin layer of emissive polymers into unclonable patterns of micron-scale islands through a brief anneal,^[20] and continued development of plasmonic scattering patterns and their analysis.^[21] Our current work expands on these contributions to establish the potential for microlens arrays integrated into the label design to simplify the detection hardware while maintaining security.

2. Results and Discussion

This section is structured as follows, we first present a fundamental proof-of-principle study using an up-conversion (UC) phosphor and laser excitation to demonstrate and characterize the working principle of the MLA-based labels. Thereafter, we establish that this label concept can be generalized to normal down-shifting (DS) phosphors and low-cost LED excitation. Finally, we discuss possible directions for further development of this label concept that would further simplify its practical implementation. For example, we briefly show how surface texturing of the label can allow excitation and detection from the same side and how this opens possibilities for a single smartphone to act as the authentication device. In this context, we also discuss the challenges and opportunities in terms of practical implementation regarding AOI control and authentication procedures.

2.1. Labels Based on Upconversion Phosphors

In the first instance, we use laser excitation and UC phosphors to rigorously test the limits of this label system. The initial concept for our label includes an MLA laminated onto a polymer layer containing UC microparticle phosphors and its authentication, as illustrated in **Figure 2**. The microlens (ML) focuses the incident 980 nm laser light into focal volumes within the microparticle-doped layer. If an UC microparticle occupies the focal volume under a given ML, bright visible emission will be observed from that point. UC phosphors have the ability to convert invisible NIR radiation to visible radiation in a non-linear manner.^[22] Hence, such UC phosphors were initially selected for the application as this nonlinearity enhances the ratio of the emission brightness of a particle within a focus to one without. However, we will later see that sufficient contrast is also easily achieved with standard down-shifting (DS) phosphors.

Figure 2a presents a schematic illustration of a prototypical implementation of our label design and an example of an authentication system. In these initial tests, a collimated excitation beam is incident on the MLA-coated side of the label. The label is held vertically on a rotation stage that controls the AOI of the excitation light. A camera (CS2100M, Thorlabs) is placed behind the label, which observes the back face of the label and captures the emitted light through an optical filter that rejects the excitation light. As mentioned previously, the precise location of this camera can be made unimportant by affine transformation of the test image relative to the reference before authentication (Section S2, Supporting Information). Figure 2b demonstrates the microscopic principle of operation

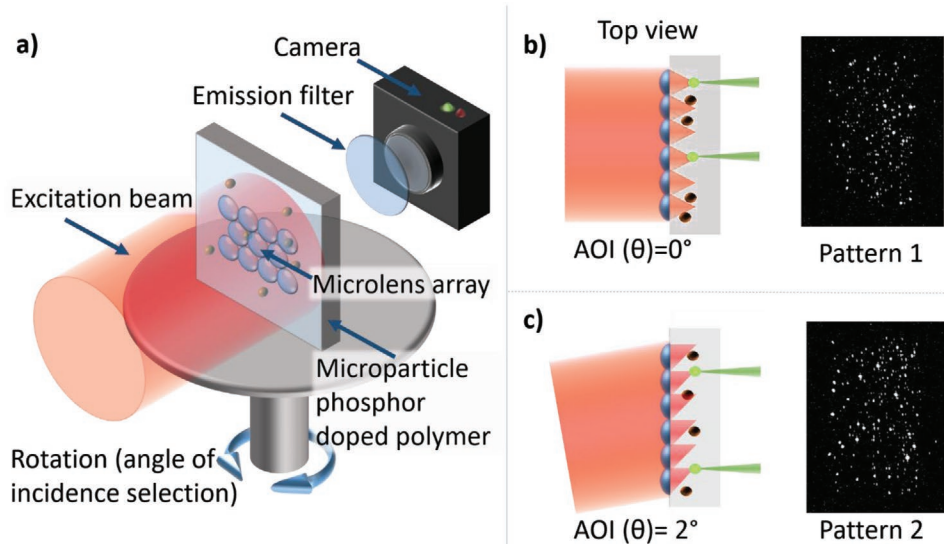


Figure 2. Illustration of the label concept with an example authentication system. a) A collimated excitation beam impinges on the microlens array and is focused into many small volumes in the phosphor microparticle-doped polymer layer. A camera collects the emission through a filter to reject the excitation light. The label is placed on a rotation stage to control the angle-of-incidence (AOI) of the excitation light. Schematic illustrations of the microscopic principle of operation and changing emission point patterns collected at an AOI of 0° (b), and 2° (c) along with example images of the different emission patterns collected from the same label at the respective AOIs.

in more detail. If a luminescent microparticle happens to lie in the focal volume of an ML, the emission from this particle is much brighter than from other particles. The emission from the microparticles is isotropic, but a certain fraction, as schematically illustrated by the green cones in Figure 2b, will escape the substrate and be collected by the camera.

As presented in Figure 2b, at normal incidence, the ML foci lie directly on the ML's center axis. This leads to a given subset of the ML foci to coincide with microparticles, and the resulting image of a constellation of bright points is labeled as pattern 1. For non-normal incidence, the foci move as indicated in Figure 2c. For collimated light, the lateral shift (x) of the foci due to a change in the AOI (θ) is given by $x = f \tan(\theta)$, where f is the focal length of the ML. The change in the position of the foci with AOI is given by $\frac{dx}{d\theta} = f \sec^2(\theta)$. For AOI close to normal $\sec^2(\theta) \approx 1$, and $dx \approx f d\theta$. For this initial demonstration with $f = 1900 \mu\text{m}$, a change in AOI of 2° led to a shift of $66 \mu\text{m}$ in the position of the foci. This is significantly larger than the $10 \mu\text{m}$ typical size of the UC microparticles (Figure S9, Supporting Information), and therefore a completely unrelated constellation is visible as now a new random set of the focal volumes overlap with different microparticles. This leads to the new point pattern as shown in Figure 2c.

To summarize the concept, our label design exploits the simplicity with which the micron-scale overlap of focal volumes under MLs and microparticles can be observed on the macroscopic scale (in terms of a bright point pattern). As the location of the focal volumes depends on the AOI of the light, the bright point pattern will change as a function of the AOI. Dependence of the emission pattern on the AOI critically enhances the security of these labels, but also determines the accuracy with which the position of the source and label must be controlled to allow reference and test images to authenticate positively at

nominally the same angle. This is an important consideration for the practical implementation of authentication systems and will be discussed in detail later.

2.2. Fabrication of Labels

We followed the procedure illustrated in Figure 3a to fabricate MLAs in photoresist on glass substrates and then placed these glass slides onto polydimethylsiloxane (PDMS) layers doped with micron-sized phosphors. Details of the two-photon lithography fabrication of the MLAs can be found in the Experimental Section with optical and SEM images of the MLAs presented in Figure 3b–d. The MLs were designed with a spherical surface (radius of curvature, ROC = $625 \mu\text{m}$), leading to a focal length, $f = Rn/(n - 1)$, of $1900 \mu\text{m}$. With the $1000 \mu\text{m}$ thickness of the glass slide, this assures that the focal volume is well contained within the $2000 \mu\text{m}$ thick PDMS layer. A $250 \mu\text{m}$ base diameter was employed for the ML, leading to a ML height of $\approx 13 \mu\text{m}$. Each MLA consisted of 240 MLs, arranged in a $5 \text{ mm} \times 3 \text{ mm}$ hexagonal array with a pitch of $250 \mu\text{m}$.

Owing to the elastomeric nature of the cured PDMS matrix, optical contact was established between the substrate and the PDMS matrix by pressing the two together (Figure 3a). In the first instance, three of these labels were fabricated for characterization using an UC phosphor to maximize the difference in emission intensity between particles within and outside of a focal volume (due to the nonlinearity of the UC emission). $\text{Gd}_2\text{O}_2\text{S}: 18\% \text{Yb}^{3+}, 2\% \text{Er}^{3+}$ was selected as the first UC phosphor. This was chosen as the UC phosphor due to the convenience of our ability to synthesize efficient material in-house by a flux-assisted solid-state method;^[23] other hosts for Yb^{3+} , Er^{3+} that support bright upconversion would also be appropriate for this application. The $\text{Gd}_2\text{O}_2\text{S}: 18\% \text{Yb}^{3+}, 2\% \text{Er}^{3+}$ phosphor is doped into the PDMS at 0.1 wt%.

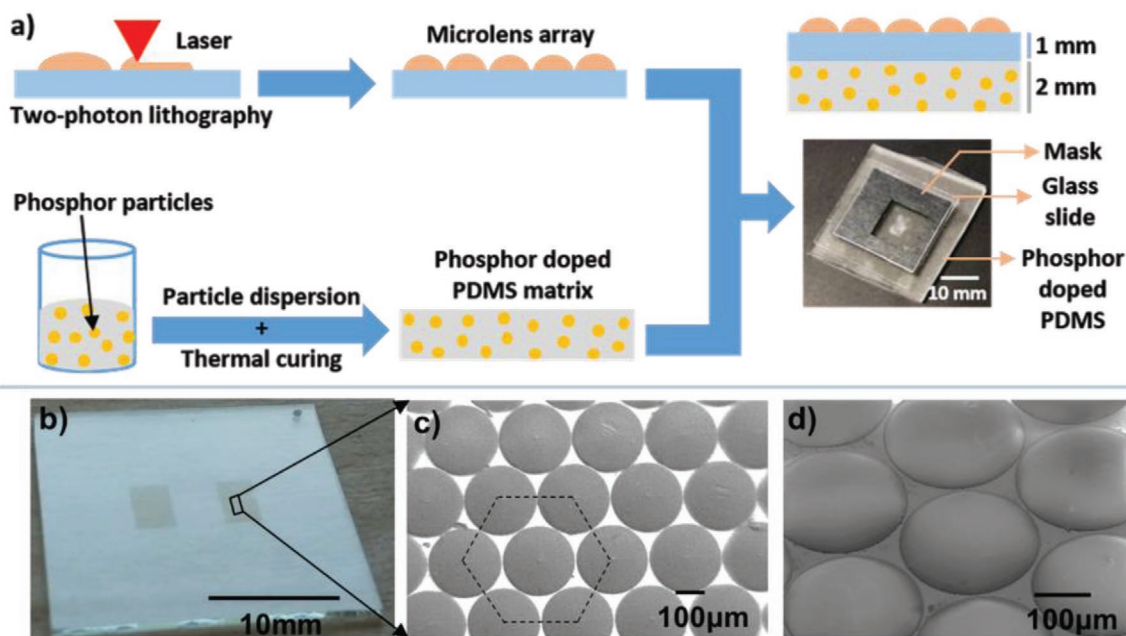


Figure 3. Label fabrication a) schematic of the label fabrication by lamination of a microlens array (MLA) on a glass substrate and then onto a phosphor doped PDMS matrix. b) Glass substrate with printed MLAs on the front surface. c) Scanning electron microscope (SEM) image of hexagonally packed MLA on the glass substrate. d) Close-up SEM image of several microlenses.

2.3. Label Characterization

The prototype UC-phosphor-based labels were characterized with a setup illustrated in Figure 2a. The MLs were illuminated using a 980 nm CW laser (SolsTiS, M2). A pair of lenses was used to expand the beam to a diameter of 10 mm. The power density of the excitation beam was 100 mW cm^{-2} . The phosphor emission was captured using a scientific CMOS camera (CS2100M-USB, Thorlabs) combined with a zoom lens (MVL7000, Thorlabs). The camera was placed 32 cm away from the label at a viewing angle of 10° with respect to the normal of the label. A 900 nm short-pass filter (FES0900, Thorlabs) was inserted before the camera to eliminate the excitation light in the capturing image. **Figure 4** presents a qualitative analysis of the similarity of the images created for the following three cases:

(i) *Trials of the Same Label at the Same Angle:* To demonstrate the reproducibility of the patterns generated by the same label under identical excitation conditions, a single label (L1) was imaged three times under normal incidence illumination. Between each image, the label was removed, and the stage rotated to a random angle. The stage was then set back to normal incidence and the label was replaced on the holder. A grayscale image is acquired from the monochrome camera for each of the three trials. Figure 4a presents these three images, along with a final comparison image in which the three images are placed into the red (R), green (G), and blue (B) channels, respectively, to form an RGB image. This RGB image highlights the reproducibility of the pattern generation. Apart from a few minor fluctuations, nearly all bright points from the three separate images coincide, leading to white points in the RGB image rather than individual colors.

(ii) *Trials of the Same Label at Different Angles:* To show the influence of the AOI, a single label (L1) was placed into the holder, and images were taken at $\text{AOI} = 0^\circ, 10^\circ,$ and 20° . As discussed above, the label should generate different bright point patterns for each AOI. These bright point-pattern images are shown in Figure 4b, alongside a final RGB composite in which each image is put into a single-color channel. In contrast to Figure 4a, no white spots appear, but rather many spots of pure colors. This is a clear representation of the uniqueness of the bright point pattern created at the different AOIs from the same label.

(iii) *Trials of Different Labels at the Same Angle:* To highlight the uniqueness of different labels (L1, L2, L3) they were placed into the holder one after the other, and each time an image was taken under normal incidence illumination. These grayscale images, as well as the RGB color composite created by placing each of these images into one color channel are presented in Figure 4c. Like Figure 4b, the bright points of single colors indicate that there is no correlation between the images and that each label is unique.

2.4. Label Authentication

The above analysis qualitatively introduces the features of our anti-counterfeiting label design. However, to understand the capabilities of these labels more quantitatively, authentication by an algorithm is necessary. Several approaches to algorithmic authentication of point patterns exist,^[24] which we adapt as follows to our specific situation, namely, to compare the similarity of the point pattern between two images (a “reference image” and a “test image”) in a way that is invariant to affine

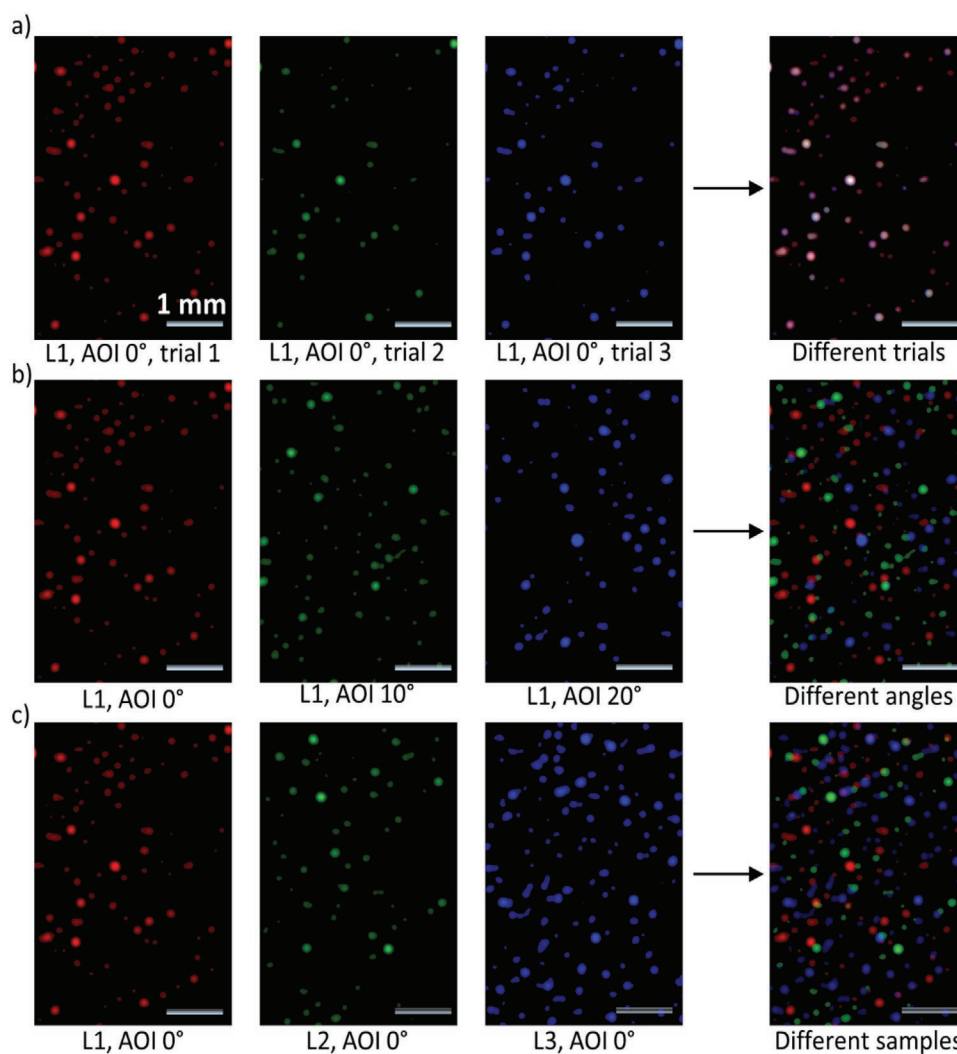


Figure 4. Qualitative comparison of point patterns observed for different labels and angles of incidence (AOIs). Red, green, blue channels for labeled conditions, and a composite image to compare the preceding three. a) Comparison of images for the same label (L1) taken under the same AOI (different trials after removing and replacing the label on the stage, images match). b) The same label (L1) under different AOIs indicated, images do not match. c) Different labels taken under the same AOI, images do not match.

transformations. A detailed description of the algorithm is presented in Section S3, Supporting Information. Briefly, the algorithm compares the reference image and test images by:

(i) *Processing an Image into a List of Points:* Each image, be it a reference or a test image, is processed to generate a list of points as follows. First, the images are binarized. This was done by finding the noise level of the image in a region outside the MLA, then assigning a value of “1” to pixels with a value greater than three times this noise level, and zero to all remaining pixels. From the binary image, contiguous bright regions are detected and enumerated. After this, the indices (x , y) of the pixel at the center of each bright spot are determined. Finally, the binarized image is used to mask the original image. Thereafter, for each bright spot, the intensity of all the pixels within the spot in the original image is summed. In the end, this process generates a sorted list of points (\mathcal{P}), in which the first point (p_1) is the index for the brightest spot and the last point (p_p) is that for the dimmest.

(ii) *Comparison of a Test Image against a Reference Image:* In the comparison phase of the algorithm, the list \mathcal{P} , obtained from the reference image, is compared to the list \mathcal{Q} , obtained from the test image. The following consideration was made: if \mathcal{P} and \mathcal{Q} originated from the same label, illuminated under the same incidence angle, an affine transformation should exist that makes $\mathcal{P} = \mathcal{Q}$. The search for such an affine transformation was adapted from Wolfson et al.^[25] We implement this concept by finding many possible affine transformations for \mathcal{Q} , of which one should be the real transformation that causes \mathcal{Q} and \mathcal{P} to overlap if the test image is from the authentic label. For each affine transformation, a vote is cast for each point in \mathcal{P} that has a point in the transformed list \mathcal{Q} within a threshold distance. The affine transformation with the most votes is considered the most suitable transformation, and this maximum number of votes is recorded and used to establish authenticity. If the number of votes is above a threshold, the reference and test images are considered to match. More details on how these

affine transformations are found and applied are provided in Section S3, Supporting Information.

To generate a set of 100 reference images, four different labels were illuminated from 25 AOIs ranging from -12° to 12° in 1° steps (the labels were of an identical design to those described in the previous section; they were based on the same MLA design and UC phosphor-doped PDMS layer). A 1° change should shift the foci by $\approx 38 \mu\text{m}$, significantly larger than the $10 \mu\text{m}$ dimension of the UC phosphor. Thus, each of these images should be uncorrelated (this is rigorously confirmed in the following section).

Then, to generate a set of 100 test images, each label was reinserted into the holder and imaged again under the same AOIs. This dataset allows 10,000 unique comparisons to be made, of which only 100 should authenticate (since the test and reference images were of the same label under the same AOI).

We applied the above algorithm to determine the number of votes cast when each test image was compared to each reference image. The following specific conditions were used in the algorithm. First, we truncated the points list to the brightest 32 points in each image for the lists P and Q . This number is found to allow robust authentication while decreasing computational costs. Second, possible affine transformations were determined by taking the five brightest points in P and Q as basis points. This number proves large enough to allow robust authentication while limiting the number of possible affine transformations to 200 (see Supporting Information for details). Third, the threshold distance for casting a vote was 15 pixels, corresponding to half the spacing of the MLs in the images. **Figure 5a** presents the number of votes cast for each reference image compared to each test image. When the test and reference image should authenticate, 24 to 30 votes are cast (this is the diagonal of the matrix shown in **Figure 5a**). For off-diagonal comparisons, a much smaller number of votes (4 to 9) are cast.

Figure 5b shows the distribution of the histograms of the number of votes cast for the 9900 non-authenticating image comparisons and the 100 authenticating ones. In each population, the number of incidences is normalized to the total number of incidences for that case, that is, the non-matching cases (yellow) are divided by 9900, and the matching cases (red) are divided by 100. This means that the total number of cases sums to one for the non-matching and matching distribution

(the area of each distribution is normalized to one). Remarkably, there is a wide separation between the number of votes cast in the matching and the non-matching cases. We now wish to select a threshold number of votes above which test image will be considered as authentic, and to estimate the rate of false-positive (and false-negative) authentications at this threshold value. To do this, the distributions of the number of votes for non-matching and matching images were fit to normalized Gaussian distributions (dashed lines in **Figure 5b**). In both cases, these Gaussian distributions are good parameterizations of the distribution of votes and will allow us to estimate the rate of false-negative or positive authentication results as a function of a threshold number of votes. The solid lines in **Figure 5b** show the cumulative distribution function (CDF) for non-matching images to obtain more than a given number of votes and the CDF for matching images to obtain less than a given number of votes. The yellow CDF, expressing the probability that non-matching images yield more than a given number of votes, can be used to estimate the probability of a false positive authentication if a given threshold is selected. For example, if a threshold of 10 votes for a positive authentication were selected, the probability of two non-matching images accidentally yielding 10 more or more votes can be read as 10^{-6} . If 14 were selected for the threshold, this probability for false-positive drops to 10^{-15} . Similarly, the probability for a false negative can be estimated from the red CDF curve that gives the probability that less than a specified number of votes are obtained from matching image pairs. In this case, if a threshold of 20 votes were selected, then the probability for a false negative would be $\approx 10^{-6}$. On the other hand, if 14 votes were selected as the threshold, the probability of a false negative match would be on the order of 10^{-15} . To minimize the sum of false positives and false negatives, the number of votes closest to the crossing point of the CDF curves should be selected as the threshold number. The curves cross at just under 14 votes. As already established, the probability that two non-matching images will generate more than 14 votes (giving a false positive match), and that the probability that two matching images have fewer votes (giving a false negative) is on the order of 10^{-15} . This statistical analysis demonstrates that robust authentication based on such labels is possible. The low chance of false positive identification also means that one test

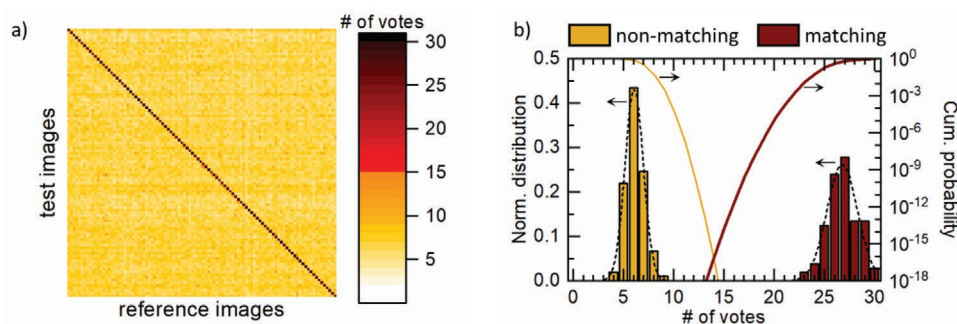


Figure 5. Label authentication. a) Maximum number of votes obtained with the used algorithm for 100 reference and 100 test images in a one-to-one comparison. b) Normalized distribution of the number of votes obtained for the ‘same’ (the same label and same angle) and ‘different’ (different label or different angle) reference and test images. The solid lines show the cumulative distribution function (CDF) for each distribution, calculated based on the Gaussian fits (dashed lines).

image could be compared against several reference images, thus relaxing the practical repositioning constraint in terms of AOI (as discussed later).

2.5. Authentication as a Function of AOI

To examine in detail the angular tolerance of the authentication of the labels discussed in the previous two sections, images were obtained for a single label at AOIs ranging from 0° to 10° in 0.1° steps. The affine-transformation-based algorithm described in the previous section was used to compare images to one another. An image, taken at a certain AOI, was used as the reference image, and all 21 images taken within an angular offset range of $\pm 1^\circ$ of the AOI image in 0.1° steps were used as test images. The resulting number of votes in these comparisons is plotted in Figure 6a. Using the authentication threshold of 14 votes, we use this data to plot the probability of authentication as a function of the angular offset in Figure 6b. As seen, reproducible authentication is only possible when the absolute angular offset is less than 0.2° . Using the authentication threshold of 14 votes, we use this data to plot the probability of authentication as a function of the angular offset in Figure 6b. On the positive side, the rapidly changing pattern with AOI leads to high security and many unique patterns. On the negative side, this necessitates an excellent control of the AOI between the label and authentication apparatus, which is challenging to maintain in the field. The main reason for this rapid change in pattern is the large discrepancy between the ML focal length of $\approx 1900 \mu\text{m}$ and the particle dimensions of less than $10 \mu\text{m}$. A 0.2° change in the incidence angle corresponds to a $7 \mu\text{m}$ change in the focus positions. As previously established, some change in pattern with AOI is critical for the security of this approach. However, such extreme angular sensitivity is not desired as it means that the positioning

accuracy of the label and excitation source need to be very high for the test image to be taken under the correct conditions.

This issue of high positioning accuracy could be addressed via two possible routes, with the goal of preserving the security introduced by angular dependence but reducing the need for highly accurate AOI control for authentication units in the field. First, a move to shorter focal length microlenses and larger microparticles will increase the range of AOIs over which a given particle remains in the focus of a microlens, and therefore increases the authentication window. An initial demonstration of this will be shown later in this manuscript in a revised label design that allows the excitation source and detector to be on the same side of the label. Thus, allowing a single smartphone for the excitation and detection through its flashlight and camera, respectively. The shorter focal length lenses in the revised design coupled with the larger particles allow authentication when the test image is taken within 3.5° of the AOI at which the reference image was captured. The physical explanation of this is as follows: as the particles become larger, the AOI tolerance is increased as the focal point created by a microlens remains within a larger particle over a wider range of AOIs. Thus, as the same microparticles remain stimulated over a wider range of AOIs, the bright point pattern remains similar for larger change in AOI. This is a critical aspect of label design, and an in-depth analysis of the role of particle size and AOI tolerance is discussed in a separate article.^[26]

A second strategy is to exploit the low probability of a false-positive authentication to introduce leeway in the accuracy to which the AOI needs to be controlled in the field by comparing a single test image to multiple reference images that are taken over a range of AOIs. Thus, the test image taken at a given (but not precisely known) AOI needs only to authenticate with one of the reference images. If the probability of a false positive for a single comparison is 10^{-15} , then the probability of a false positive after n comparisons can be expressed as:

$$P = 1 - \left(\frac{10^{15} - 1}{10^{15}} \right)^n$$

Hence, if a single test image were compared with 10 or 100 reference images, the probability of a false positive would only increase to 10^{-14} or 10^{-13} , respectively (the false positive rate increasing linearly with n in this regime of the number of trials being much smaller than the false positive rate). Running on a desktop computer (Intel Core i5-3470, 3.2 GHz processor), the 10,000 test-reference comparisons shown in Figure 5 took 2056 s to complete, meaning the average time taken to compare a test and reference was 0.2 s. Therefore, 2 or 20 s would be needed to compare a single test image with 10 or 100 reference images over a range of angles. For the extremely sensitive case above, reference images would need to be taken every 0.2° , so comparison with 10 or 100 images would allow the effective positioning accuracy needed for the AOI in field devices to be decreased to $\pm 1^\circ$ or $\pm 10^\circ$. The cost in terms of the false-positive rate is still within acceptable limits. Further, with the appropriate development of the authentication algorithm, the time necessary for authentication should also be reduced. In terms of algorithm development, currently 200 separate possible affine transformations are considered for each test-reference comparison; this should be possible to reduce. One example of a strategy to reduce the number of tested affine transformations

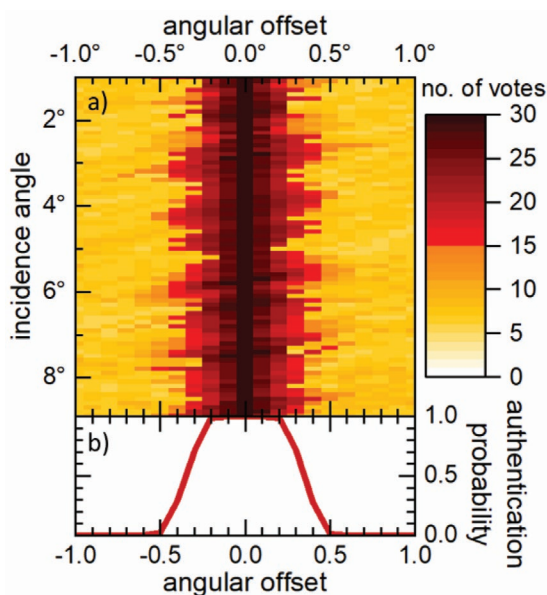


Figure 6. a) Number of votes for test images with given offsets in angle of incidence compared to a reference image. b) Probability of authentication as a function of the offset in angle of incidence between the test and reference image (based on a threshold of 14 votes).

is to estimate the label's pose relative to the camera through fiducial markers on the surface of the label. We also note that such a reduction in the number of affine transformations of the test image compared to the reference image should reduce the false positive probability thus, counteracting comparing the test image to an increased number of reference images.

2.6. Labels Based on Down-Shifting Phosphors

The results presented in the preceding section utilized UC phosphors in the label design. These labels required excitation from a high-intensity source and a monochrome 16-bit scientific camera with a zoom lens (MVL7000 – 18 – 108 mm EFL, Thorlabs) was used for detection. In this section, we demonstrate that labels based on standard DS phosphors can enable authentication using an inexpensive light-emitting diode source and a standard smartphone camera. To prepare these labels, the same MLAs of ($f=1900\ \mu\text{m}$) and PDMS layers were used as before. However, the PDMS was doped with commercially available DS particles (YYG 557 230 isiphor) at a concentration of 0.5 wt%. This DS phosphor can be excited with a blue LED (excitation peak at 450 nm) and emit in a broad visible wavelength range of 470 to 700 nm. The particles have a D50-particle size of 30.5–34.5 μm . The excitation, emission, and diffuse reflection spectra alongside SEM images of the phosphor are presented in Sections S4 and S5, Supporting Information. YYG 557 230 isiphor was selected due to the ease of its commercial availability, but other downshifting microphosphors with respectable brightness are equally appropriate for this application.

Figure 7a,b presents the images of this label under illumination with a 450 nm LED at 0° AOI taken with the scientific CMOS camera and a smartphone (Samsung galaxy A71) both placed behind the label. In Figure 7 the images have been binarized and registered to one another using an affine transformation (to account for the different perspectives of the cameras, see below for details). The full geometry of the setup is explained in Section S6, Supporting Information. A key obser-

vation is that the contrast between the emission intensity of DS microparticles inside versus outside a ML focal volume is sufficient that a bright point pattern is clearly resolved. The second observation is that the smartphone (8-bit color image) and scientific CMOS camera (16-bit monochrome image) record the same bright point pattern. Although the smartphone camera does not require any additional lens to resolve the bright point pattern, we note that an emission filter is needed to filter out the excitation light. For a quantitative comparison, analyzing the images presented in Figure 7a,b with our authentication algorithm results in 27 votes being cast. This is far greater than the threshold of 14 votes, indicating that the algorithm also considers these images to be an identical match. To visually demonstrate the equivalency of the camera images, the affine transformation related to this largest number of votes was applied to the smartphone image and then a false-color image of the CMOS captured image (green) together with the transformed smartphone image (magenta) was generated and is presented in Figure 7c.

2.7. Label Authentication Using a Single Smartphone

In the previous section, we demonstrated that labels based on DS phosphors are possible and that a smartphone camera can image the bright point pattern using 450 nm LED excitation. Interestingly, the flashlight in smartphones also has a peak emission at 450 nm. Hence, we hypothesize that it should be possible to excite and detect such labels using a single smartphone. However, to do this the excitation and detection need to be done on the same side of the label. This requires the label to be redesigned, as the close-packed microlens in the above design distort (collimate or focus) the emission of the microparticles that propagates back in the direction of the excitation source.

For the label to work in a “reflection” geometry (with the source and detector on the same side of the label) the following are necessary: 1) increasing the spacing of the microlens array

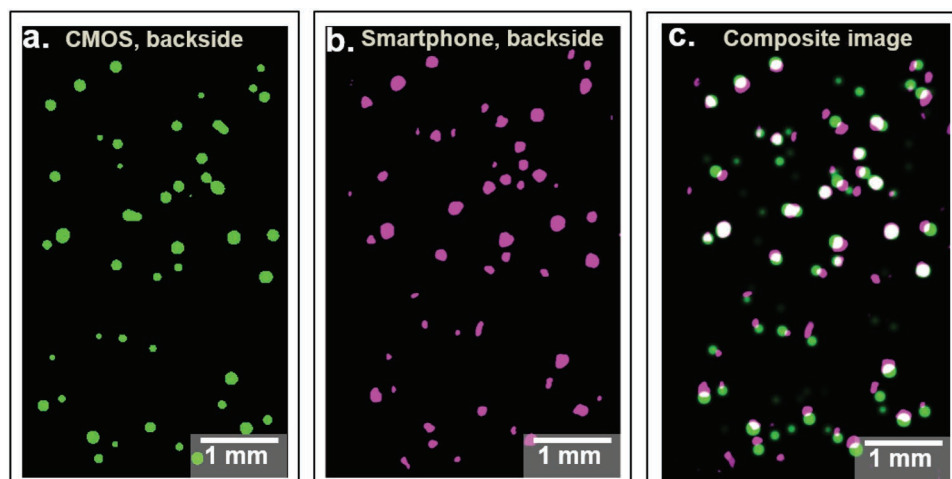


Figure 7. Unclonable label based on standard down-shifting phosphor allows authentication using LED excitation and smartphone detection. a) DS phosphor pattern observed by the s-CMOS camera. b) DS pattern observed by a smartphone camera. c) Composite zoom-in image of CMOS (reference) and smartphone-captured image in a single frame after an affine transformation.

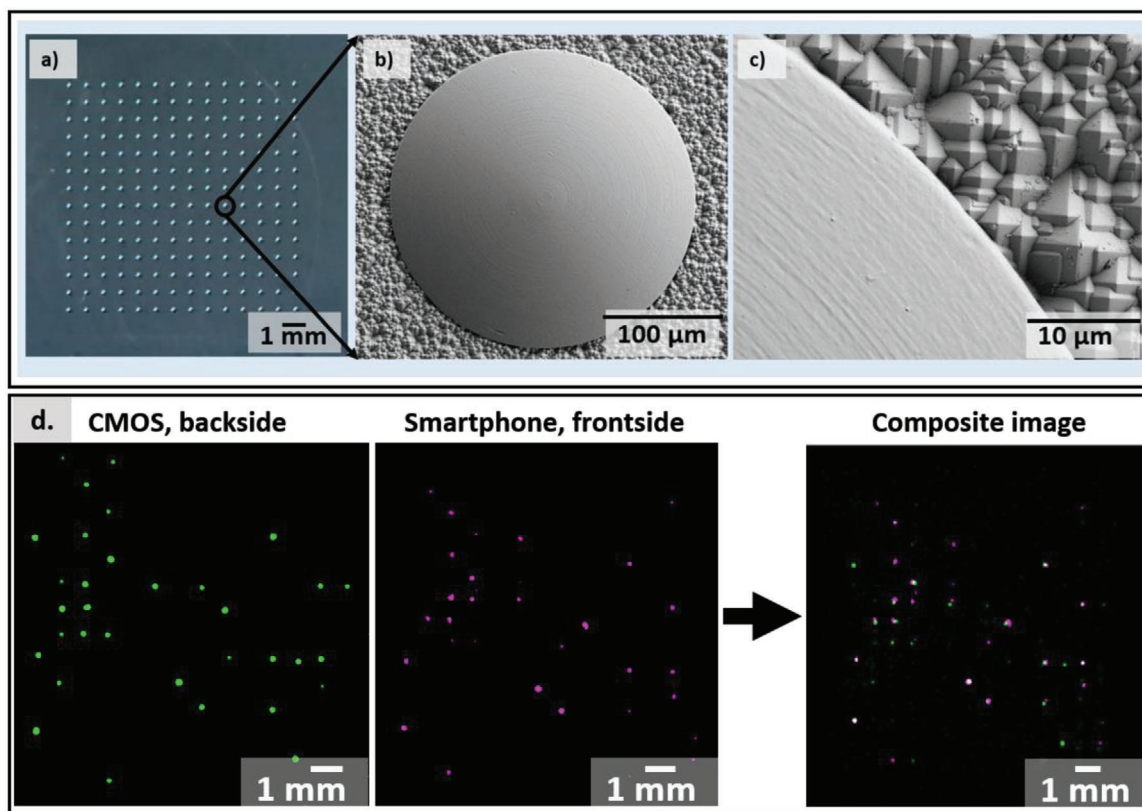


Figure 8. Unclonable label that can be excited and read-out by a single smartphone (on the front-side). Figure 8 (a–c) shows the optical and SEM images of the MLA master on the textured Si substrate. d) The DS pattern observed at the backside of the label by a CMOS camera and by the smartphone camera also providing the illumination (front side). The composite image shows the similarity of the patterns captured from the two devices. The authentication algorithm yields 21 votes for the two images which is well above the threshold of 16 determined for these labels (see text).

so that light emitted from a bright particle hits the substrate surface between the microlenses; and 2) adding a scattering texture to the front surface of the label between the microlenses to better couple this light back to the camera (rather than it undergoing total internal reflection). **Figure 8a–c** presents optical and SEM images of this new MLA design. For this label, we have implemented a 14×14 MLA having a focal length of $550 \mu\text{m}$ (ROC $200 \mu\text{m}$, base diameter $250 \mu\text{m}$) and distributed in a square-packing arrangement with a center-to-center distance of $750 \mu\text{m}$. The fabrication procedure is slightly more elaborate than for the previous MLAs. In this case, a positive master of the label surface is made by a two-photon lithography to create the microlens array on the surface of a structured silicon substrate. The silicon substrate is a $\langle 100 \rangle$ -oriented silicon wafer that underwent an anisotropic chemical etch to expose the $\langle 111 \rangle$ -planes, exhibiting the characteristic pyramidal micro-texture (supplied by Amonix Inc. USA). This design is then replicated into PDMS to form a stamp with the negative of the desired surface texture. Finally, a layer of UV-curable optical adhesive is distributed on the surface of a $400 \mu\text{m}$ glass slide, stamped with the PDMS, and finally cured. This results in the MLA and scattering pyramids on the glass substrate that is then laminated to a microphosphor-doped PDMS layer (full details of fabrication can be found in Section S7, Supporting Information). In this case, the PDMS layer was doped with 0.5 wt% DS phosphor (YYG-557-230 isiphor) microparticles.

This new label was tested as follows. At the front side of the label (MLA side), a smartphone placed 10 cm away from the label provides illumination at an AOI of 10° . This excitation light is passed through a 500 nm short-pass filter (FES0500, Thorlabs) to remove the longer wavelength components of the white flashlight that would otherwise interfere with the detection of the emitted light. The bright-point images are simultaneously captured at the front (by the same smartphone) and at the back (by the scientific-CMOS camera, 32 cm away and 10° off the optical axis). Both cameras are covered with 500 nm long-pass filters to reject the excitation light (FEL0500, Thorlabs). A schematic is provided in Section S9, Supporting Information.

Figure 8d shows the binarized images of the point-patterns captured by the CMOS camera (green) and by the smartphone camera (magenta). To compare the patterns, the smartphone image was mirrored to match the CMOS image taken from the other side of the label, and an affine transformation based on three equivalent points in each image was used. In the composite image, a clear correlation is visible between the pattern detected by the smartphone on the front-side and that detected by the CMOS camera on the backside. For more quantitative analysis, we need to first determine the threshold number of votes for this new label design. To do this, we return to a similar analysis as that presented in **Figure 5**. In this case, we prepare four separate labels and record images at AOIs from -25° to 25° with a step of 10° (6 angles). The wider spacing of

the angles as compared to the data in Figure 5 is because the images remain correlated for a greater range of AOIs in this new design. Nonetheless, a step of 10° is sufficient such that entirely different patterns are generated even. This is qualitatively presented in Section S8, Supporting Information. Hence, in this case, we compare each of the 24 reference images with each of the 24 separate test images (taken after removing and replacing the sample and following the same procedure as above). Of these 576 comparisons, 24 should authenticate (same label, same AOI), whereas the remainder should not. The vote distributions are shown in Section S8, Supporting Information, with the matching and non-matching populations well separated with on average 30 votes cast for 24 test–reference pairs that should authenticate, and an average of 4 votes cast for the test–reference pairs that should not authenticate. In this case, an analysis of the two distributions allows us to estimate a threshold for authentication of 16 votes. 21 votes are cast upon comparing the two images shown Figures 8a and 8b, which is well above the threshold for authentication. This is an initial demonstration that authentication based on a single smartphone is feasible with front side excitation and detection.

We also note that owing to a larger particle size and a shorter focal length lens, the range of AOIs over which a test and reference image authenticate for this label design is greater than that of the previous design. Upon subjecting the new label to a similar analysis as presented in Figure 6, it is observed that a test image will authenticate with the reference if the test is taken within 3.5° AOI of the reference image. Complete details for the same are provided in Section S8, Supporting Information. Thus, the new label design confirms that particle size and focal length can be controlled to influence the AOI range over which authentication is possible. Further understanding of this topic is explored more thoroughly in a separate upcoming study.

3. Discussion

The labels presented here combining microlens arrays with the microparticles allow the micron-scale randomness to be readily imaged on the macroscale and are potential alternatives to labels based on a more direct observation of micron-scale randomness.^[19] In terms of practical implementation, our initial prototype labels are mainly based on small ($10\ \mu\text{m}$) UC phosphor particles and closely packed MLAs with a long focal length ($1900\ \mu\text{m}$). These labels require a transmission geometry and can only authenticate images taken with less than 0.2° difference of AOI to the reference. This means that they act more as a proof of concept, rather than being ready for widespread commercial use. Nonetheless, an example of a specific use case for these proof-of-concept labels would be the authentication of medication in blister packs. In this case, the microlens and phosphor doped layer could be placed on opposite sides of the transparent blister pack substrate, or eventually the phosphors could be incorporated into the polymer packaging material and the microlens array imprinted onto it. The blister pack could then be inserted into authentication hardware against fixed guides and stops to accurately control the position of the blister pack on a transparent bed (like a document scanner). Three or more separate LEDs under the bed could provide illumination at

accurate (and fixed) AOIs. A camera above the blister pack could image the constellation of bright emission points for each LED excitation. This would be a specific example in which control of the AOI in the field authentication units should be possible to maintain. Also in this example, LEDs of different wavelengths could be used. This would allow labels to be made with the additional security of excitation-dependent emission.^[27] For example, if both UC phosphor particles and DS phosphor particles were doped into the label, the point pattern observed would depend on whether NIR or visual excitation was used (these wavelengths exciting only the UC or DS particles respectively), and this would add another possible level to the label security.

Ultimately, the ability to label a variety of goods, including those with curved surfaces, is of key importance for unclonable labels.^[20] Given the use of a glass substrate for the microlens array, the prototype labels used to demonstrate the general concept herein are not yet well suited to such an application. The further development of this concept to use a single flexible polymer layer in which the microparticles are doped and onto which the microlens array is imprinted is a direct (and feasible) target that would allow the transfer of the complete label onto a product. In terms of marking curved products, we note that the angle of incidence of collimated incoming light will vary

as $\Theta = \frac{180x}{\pi R}$, where R is the radius of curvature of the marked

object, and x is the arc length between point on the label that is closest to the illumination source, and the microlens in question. For example, for a radius of curvature of 3 cm (a perfume bottle for example) and a label length of 2 cm, the AOI would vary from 0° for microlenses in the center of the label to $\Theta = \frac{180}{3\pi} \approx \pm 20^\circ$ for microlenses at the outer edges of the label.

If the radius of curvature stays constant, and the reference images are taken of the labels in place on the product, then labels of this concept should be applicable to curved surfaces. To mark objects that are flexible with labels of this concept will require careful consideration. The AOI changes with the radius of curvature of the object, so if a flexible object is marked it must be brought into the same configuration (i.e., flat) for taking the test image as it was in when the reference image was taken. Although challenges clearly remain to market-ready application, these initial results are of sufficient promise to stimulate further development to meet these challenges.

Also, the ability to perform authentication with a single smartphone would be greatly enhance the number of use cases. The single smartphone means that excitation and detection must both be done from the front side of the label. We have made the first steps in this direction by modifying the spacing of the MLAs and incorporating a surface texture to outcouple light in order that a single smartphone can be used to excite and detect the constellation of bright emission at the front side. Currently, filters for both excitation and emission are needed to block unwanted wavelengths at the source and detection points, respectively. Also, it would be preferable that the smartphone be held by hand, or in a simple mechanical apparatus. For authentication to be possible in such cases, a further reduction in the AOI positioning accuracy must be pursued. Promising routes in terms of label design involve moving to shorter focal length lenses and larger particles. These may need to be

complemented by development of the ability to estimate the position of the label relative to the phone by fiducial markings to work out the AOI, and/or by comparing a single test image against a number (e.g., 10 or 100) of reference images that are taken over a range of AOIs. Removing the need for filters in front of the flashlight and camera by better dealing with scattered light in the label design is also an important direction for future work.

To bring these prototypes to practical application, further work must also target the increase in stability of the labels. The photostability of the phosphors is not anticipated to be a problem. Indeed, the brightness of the points from the DS phosphor did not noticeably decrease in brightness over 6 months' time (see Section S8, Supporting Information). Furthermore, given this concept will work with a wide variety of microphosphor particles and polymer layers, guidance from the lighting community (e.g., from phosphor-converted light-emitting diodes^[28]) should be useful in choosing highly photostable combinations of microphosphor and polymer host. The major challenge to reproducible long-term authentication in the current prototype design is the shift with aging between the PDMS layer loaded with the microphosphor particles and the glass layer on which the microlens array is made. In this prototype design, these layers are not bonded together. Gradual slip between the glass slide that the microlens array is fabricated on, and the underlying microphosphor-doped polymer layer will cause the point pattern produced to gradually change with time, and the label to stop authenticating against the originally taken reference images. Revised label designs will be explored to overcome this challenge in which the microlens layer is bonded to the polymer layer, or the microlens are directly embossed into the polymer layer.

4. Conclusion

We have introduced a concept for anti-counterfeiting labels based on a combination of microlens array and a polymer layer doped with microphosphor particles. The constellation of bright emission points generated by these labels vary with the angle of the illumination as different subsets of microparticles coincide with the microlens foci as these shift with the AOI. The constellation of bright emission points can be imaged with standard digital cameras (such as those of smartphones). By utilizing several different constellation patterns taken at different AOIs for authentication, these labels become effectively unclonable. Compared with the approach of Pappu et al. based on scattering of coherent radiation,^[7] our design has two critical advantages in terms of practical implementation in that it allows standard LEDs to be used as the excitation source and the generated macroscopic pattern does not depend on the detector location. We also demonstrate that these features allow a single smartphone to be used for authentication (albeit currently still requiring an optical filter over both the camera and the LED). By making the micron scale randomness readily accessible on the macroscale, this new concept for unclonable labels offers an interesting challenger to label concepts that rely on magnification in the authentication hardware. With the increasing need to identify products securely and uniquely, we anticipate fruitful further development of both these concepts.

5. Experimental Section

Fabrication of Microparticle Layers: First, the desired weight percentage of phosphor particles was dispersed in the silicone elastomer base (SYLGARD 184, Dowsil, RTV-A). A high-speed dispersion device (CAT M. zipper GmbH) was used to disperse phosphor particles uniformly in the RTV-A solution. Then, the curing agent (RTV-B) was mixed throughout the solution with a component ratio RTV-A:RTV-B of 10:1. The resulting solution was kept in a vacuum desiccator to extract air bubbles from the mixture. The mixture was then poured in a 2 mm thick polished brass mold and cured at 150 °C for 30 min in an open-air environment, the authors note that this elevated temperature was chosen to more rapidly cure the PDMS layers (and layer so produced maintain good optical quality). The phosphor particles do not hinder the curing of the PDMS and longer curing times at lower temperatures can also be used.

Gadolinium oxysulfide doped with an ytterbium sensitizer (980 nm absorption) and a visible erbium emitter ($\text{Gd}_2\text{O}_3\text{:S: 18% Yb}^{3+}$, 2% Er^{3+}) was used as the UC phosphor. It was prepared in-house via a flux-assisted solid-state method as described by Katumo et al.^[23] The characteristic particle size of UC phosphor was in the order of 10 μm and exhibits rod-like morphology as demonstrated in Section S5 and Figure S9, Supporting Information. The DS phosphor was the commercial YG 557 230 isophor (Merck). This was a cerium-activated aluminum-garnet yellow phosphor, in a spherical shape with a D50 particle size between 30–35 μm as demonstrated by the SEM image shown in Figure S9 and Section S5, Supporting Information.

Fabrication of Microlens Arrays: The MLA was designed in Matlab (MathWorks) and printed using a Photonic Professional GT (Nanoscribe) on a 1 mm thick glass substrate coated with indium tin oxide (ITO). The resist used to fabricate MLA was IP-S (Nanoscribe). As the refractive indices of IP-S resin and the glass substrate were nearly the same, it was difficult for the device to find the interface print position between the glass and IPS. Therefore, it was recommended to use an indium tin oxide (ITO)-coated glass substrate with the IP-S photoresin for the 3D micro-texture writing. The authors printed 240-elements MLA which were distributed in a hexagonally close-packed manner (for the UC phosphor doped label). The MLA took roughly 30 h to print.

Hardware Setup: For observing the visible UC emission, a full-high-definition (FHD) CMOS camera (CS2100M, Thorlabs) with an 18–108 mm zoom lens was used (MVL7000 – 18 – 108 mm EFL, Thorlabs) set to a focal length of 108 mm. The camera was placed behind the polymer sample, facing the back surface of the label at 32 cm. The camera was placed 10° off the optical axis to avoid transmitted laser light. A 2.5 cm diameter 900 nm short-pass filter (FES0900, Thorlabs) was centered directly in front of the 5.4 cm diameter opening of the lens using a blocking aperture to further reject excitation light. A technical schematic showing the positions and angles of the incident beam, label, filter, and the camera is presented in Section S10, Supporting Information. To illuminate the MLA surface area with the collimated and expanded version of the laser beam, the beam profile of the excitation beam was expanded using a pair of lenses having focal lengths of –25 and +100 mm, respectively. The label was mounted on a motorized rotational stage (CR1/M-Z7, Thorlabs), which itself was fixed on an X–Y stage. The illumination area on the label, that is, the MLA region was made to place at the center of the rotational axis such that each microlens faces the same AOI while rotating the label stage.

In the smartphone reading setup (Figure S10, Supporting Information), a Samsung galaxy A71 was used. The smartphone camera was covered with a 500 nm long-pass filter (FEL0500, Thorlabs) by taping the filter holder directly over the smartphone camera. The smartphone was positioned 10 cm behind the sample, with an angle of $\Phi \approx 10^\circ$ to the optical axis. In the setup for smartphone excitation and detection (Figure 8a), the same smartphone was used but the flashlight was covered with a 500 nm short-pass filter (FES0500, Thorlabs), in addition to the filter over the camera. In this case, the filter over the camera was slightly raised, as it was stacked on top of the filter over the flashlight. The distance of the smartphone while capturing the emission-based image from the

label was 10 cm and the flashlight was aligned to point directly at the center of the label.

An open-source camera app named Open Camera (v1.48.1 code 77), available in the Google Play store was used to capture the label's bright pattern from the smartphone. The app provides a user interface platform called Application Programming Interface (API) to manually control the functions of the smartphone camera. For this, the default setting (original camera API) had been changed to a manual setting, called "Camera2API". In this manual mode, the authors had changed the camera settings to capture the label pattern as follows: the spatial resolution was set to 4032 × 3024 pixels. The focus distance was set to 10 cm, the white balance was set to fluorescent, the color effect to none, and then the auto level to unchecked. The focus region of the bright point pattern on the label was digitally zoomed in 6× times to the smartphone screen. The ISO was manually set to 800 and locked at this value to lower the noise in the capturing image. The exposure time was set to 1/30 s and locked. All these settings were saved and could be retrieved during the time of re-use in the setting manager of the application.

Supporting Information

Supporting Information is available from the Wiley Online Library or from the author.

Acknowledgements

The authors gratefully acknowledge the Helmholtz Association for funding through HEMF, KNMF, and the MTET program (Materials and Technologies for the Energy Transition) – Topic 1 – Photovoltaics (38.01.05), and the recruiting initiative of B.S.R. The authors V.K. and N.K. acknowledge the DAAD for financial support. The authors thank Arndt Last at the Institute of Microstructure Technology, KIT for his technical support with the photograph in Figure 1.

Open access funding enabled and organized by Projekt DEAL.

Conflict of Interest

The authors have filed a patent application and are pursuing the commercial application of this technology.

Data Availability Statement

The data that support the findings of this study are available from the corresponding author upon reasonable request.

Keywords

anti-counterfeiting, microlens arrays, microphosphors, physical unclonable labels, smartphone authentication, threshold votes

Received: November 5, 2021

Revised: February 10, 2022

Published online:

- [1] P. Strykowski, M. Gaudiau, M. Kazimierzczak, N. Wajzman, *Illicit Trade—Global Trade in Fakes: A Worrying Threat*, OECD Publishing (OECD/EUIPO), Paris **2021**.
- [2] Frontier Economics, *The Economic Costs of Counterfeiting and Piracy*, Report prepared for BASCAP and INTA, <https://www.iccwbo.be/wp-content/uploads/2017/06/ICC-BASCAP-Frontier-report-2016-Executive-Summary.pdf> (accessed: May 2021).

- [3] a) P. Aldhous, *Nature* **2005**, *434*, 132; b) Y. Gu, C. He, Y. Zhang, L. Lin, B. D. Thackray, J. Ye, *Nat. Commun.* **2020**, *11*, 516.
- [4] J. Stradley, D. Karraker, *IEEE Trans. Compon. Packag. Technol.* **2006**, *29*, 703.
- [5] R. Arppe, T. J. Sørensen, *Nat. Rev. Chem.* **2017**, *1*, 0031.
- [6] a) Y. Gu, C. He, Y. Zhang, L. Lin, B. D. Thackray, J. Ye, *Nat. Commun.* **2020**, *11*, 516; b) M. R. Carro-Temboury, R. Arppe, T. Vosch, T. J. Sørensen, *Sci. Adv.* **2018**, *4*, e1701384.
- [7] R. Pappu, B. Recht, J. Taylor, N. Gershenfeld, *Science* **2002**, *297*, 2026.
- [8] W. Ren, G. Lin, C. Clarke, J. Zhou, D. Jin, *Adv. Mater.* **2020**, *32*, 1901430.
- [9] a) J. D. R. Buchanan, R. P. Cowburn, A.-V. Jausovec, D. Petit, P. Seem, G. Xiong, D. Atkinson, K. Fenton, D. A. Allwood, M. T. Bryan, *Nature* **2005**, *436*, 475; b) P. R. Seem, J. D. Buchanan, R. P. Cowburn, *Opt. Lett.* **2009**, *34*, 3175; c) B. Wigger, I. Koinzer, T. Meissner, M. Barth, A. Zimmermann, *Robot. Comput. Integr. Manuf.* **2020**, *63*, 101925; d) C. Yeh, C. Lee, C. Lin, *IEEE Trans. Ind. Inf.* **2015**, *11*, 505; e) E. Toreini, S. F. Shahandashti, F. Hao, *ACM Trans. Privacy Secur.* **2017**, *20*, 9.
- [10] B. Wigger, T. Meissner, A. Förste, V. Jetter, A. Zimmermann, *Sci. Rep.* **2018**, *8*, 4738.
- [11] T. Takahashi, Y. Kudo, R. Ishiyama, Fifteenth IAPR International Conference on Machine Vision Applications (MVA), **2017**, pp. 202–206, <https://doi.org/10.23919/MVA.2017.7986836>.
- [12] R. Ueno, J. Mitsugi, presented at 2018 IEEE 4th World Forum Internet Things (WF-IoT), **2018**, pp. 416–420.
- [13] J. Kim, J. M. Yun, J. Jung, H. Song, J.-B. Kim, H. Ihee, *Nanotechnology* **2014**, *25*, 155303.
- [14] H. J. Bae, S. Bae, C. Park, S. Han, J. Kim, L. N. Kim, K. Kim, S.-H. Song, W. Park, S. Kwon, *Adv. Mater.* **2015**, *27*, 2083.
- [15] Y. Zheng, C. Jiang, S. H. Ng, Y. Lu, F. Han, U. Bach, J. J. Gooding, *Adv. Mater.* **2016**, *28*, 2330.
- [16] A. F. Smith, P. Patton, S. E. Skrabalak, *Adv. Funct. Mater.* **2016**, *26*, 1315.
- [17] Y. Liu, F. Han, F. Li, Y. Zhao, M. Chen, Z. Xu, X. Zheng, H. Hu, J. Yao, T. Guo, W. Lin, Y. Zheng, B. You, P. Liu, Y. Li, L. Qian, *Nat. Commun.* **2019**, *10*, 2409.
- [18] J. W. Leem, M. S. Kim, S. H. Choi, S.-R. Kim, S.-W. Kim, Y. M. Song, R. J. Young, Y. L. Kim, *Nat. Commun.* **2020**, *11*, 328.
- [19] R. Arppe-Tabbara, M. Tabbara, T. J. Sørensen, *ACS Appl. Mater. Interfaces* **2019**, *11*, 6475.
- [20] N. Kayaci, R. Ozdemir, M. Kalay, N. B. Kiremitler, H. Usta, M. S. Onses, *Adv. Funct. Mater.* **2021**, <https://doi.org/10.1002/adfm.202108675>.
- [21] a) J. D. Smith, M. A. Reza, N. L. Smith, J. Gu, M. Ibrar, D. J. Crandall, S. E. Skrabalak, *ACS Nano* **2021**, *15*, 2901; b) Q. Li, F. Chen, J. Kang, J. Su, F. Huang, P. Wang, X. Yang, Y. Hou, *Adv. Funct. Mater.* **2021**, *31*, 2101537; c) M. Ibrar, S. E. Skrabalak, *Small Struct.* **2021**, *2*, 2100043.
- [22] M. Pollnau, D. R. Gamelin, S. Lüthi, H. Güdel, M. P. Hehlen, *Phys. Rev. B* **2000**, *61*, 3337.
- [23] N. Katumo, G. Gao, F. Laufer, B. S. Richards, I. A. Howard, *Adv. Opt. Mater.* **2020**, *8*, 2000507.
- [24] a) S. M. Elshoura, D. B. Megherbi, *Signal Process. Image Commun.* **2013**, *28*, 531; b) T. Wakahara, Y. Kimura, A. Tomono, *IEEE PAMI* **2001**, *23*, 384; c) V. Monga, D. Vats, B. L. Evans, *IEEE Int. Conf. Multimedia Expo*, **2005**, pp. 229–232.
- [25] H. J. Wolfson, I. Rigoutsos, *IEEE Comput. Sci. Eng.* **1997**, *4*, 10.
- [26] V. Kumar, S. Dottermusch, A. Chauhan, B. S. Richards, I. A. Howard, *Adv. Photonics Res.* **2022**, <https://doi.org/10.1002/adpr.202100202>.
- [27] H. Suo, Q. Zhu, X. Zhang, B. Chen, J. Chen, F. Wang, *Mater. Today Phys.* **2021**, *21*, 100520.
- [28] G. B. Nair, H. C. Swart, S. J. Dhoble, *Prog. Mater. Sci.* **2020**, *109*, 100622.